Chemical Engineering Journal 507 (2025) 160639

Contents lists available at ScienceDirect

Chemical Engineering Journal

journal homepage: www.elsevier.com/locate/cej

Waste lignosulfonate upcycling towards durable and efficient pelletized adsorbents for diluted NH_3 adsorption

Guo-Wen Fang [a], Zhang-Min Li [a,*], Jian-Fei Li [a], Dan-Dan Cai [a], Yu-Jie Xiong [a], Yan Zhou [a], Wei Hui [a,b,**], Duan-Jian Tao [a,*]

[a] National Engineering Research Center for Carbohydrate Synthesis, Key Laboratory of Fluorine and Silicon for Energy Materials and Chemistry of Ministry of Education, School of Chemical Engineering, Jiangxi Normal University, Nanchang 330022, China
[b] School of Life Science, Jinggangshan University, Ji'an 343009, China

ARTICLE INFO

Keywords:
Industrial lignin waste
Paper pulp
Sodium lignosulfonate
Diluted NH_3 adsorption
DFT

ABSTRACT

Lignin is the largest natural reservoir of aromatic compounds while its intricate polymeric structure complicates the reuse of lignin-derived waste. Herein, we report the development of lignin-based NH_3 adsorbents by upcycling sodium lignosulfonate (SLS) from spent paper pulp liquor. The demethylation of SLS was carried out to obtain the demethylated SLS (DSLS) and subsequently the pelletized DSLS@binder adsorbents were prepared using DSLS and three binders. The results indicate that the optimized 95% DSLS@PVA pellets with binder dosage of 5 wt% PVA (polyvinyl alcohol, PVA) exhibit the NH_3 adsorption capacity of 11.5 mmol g^{-1}, along with remarkable selectivity uptake for NH_3/N_2 (3573) and NH_3/CO_2 (1380). Moreover, the 95% DSLS@PVA pellets demonstrate ultra-fast adsorption kinetics (half-capacity uptake time of merely 38 s). Column breakthrough tests showed that the 95% DSLS@PVA pellets achieved NH_3 retention time of 370 min g^{-1} in a ternary gas mixture of $NH_3/N_2/CO_2$ (1 %/98 %/1%), with a dynamic adsorption capacity of 2.07 mmol g^{-1}. In addition, the 95% DSLS@PVA has a good balance between mechanical strength and NH_3 uptake cycle performance. This work provides a sustainable strategy for valorizing lignin waste into high-performance NH_3 adsorbents.

1. Introduction

Industrial production, while supporting societal development, inevitably generates waste materials and pollutants that pose environmental challenges. For example, ammonia (NH_3) emissions from industrial chemical synthesis processes (e.g., fertilizers, pharmaceuticals, explosives) and lignin waste from the paper industry are major sources of by-products [1]. It is estimated that industrial activities worldwide release $>$ 10 million tons of NH_3 exhaust gases annually, which contributes to significant environmental burdens [2–4]. Similarly, the global yearly output of lignin waste, such as sodium lignosulfonate (SLS), a by-product of paper pulp liquor, is estimated at around 1.8 million tons, which accounts for ~90 % of the total commercial market [5]. The toxicity and corrosive nature of these wastes contribute to air and water pollution, damage ecosystems and pose a public health risks [6,7]. In this context, the principles of green and sustainable chemistry emphasize the potential to convert waste materials into valuable resources. Therefore, the sustainable reuse of waste SLS as an NH_3 adsorbent offers a novel perspective for resource recycling with significant practical value.

Waste SLS contains functional groups such as phenolic hydroxyl, alcoholic hydroxyl, and methoxy groups, which endow it with specific chemical activity. Given the basic nature of NH_3, adsorbents with acidic sites have been widely explored as an NH_3 capture strategy. Notably, methoxy group can be demethylated to form weakly acidic phenolic hydroxyl groups [8], which renders demethylated SLS (DSLS) a promising candidate for selective NH_3 capture. Therefore, DSLS has great promise to be a sustainable alternative to conventional NH_3 adsorbents. It is noteworthy that the industrial standard for high-throughput gas separation using pressure swing adsorption (PSA) requires durable and moldable adsorbents with rapid mass transfer kinetics, high adsorption capacity and selectivity [9,10]. To meet industrial demands, various adsorbents have been developed for NH_3 separation, such as activated carbons [11–14], zeolites [15,16], metal–organic frameworks (MOFs)

---

* Corresponding authors.
** Corresponding author at: National Engineering Research Center for Carbohydrate Synthesis, Key Laboratory of Fluorine and Silicon for Energy Materials and Chemistry of Ministry of Education, School of Chemical Engineering, Jiangxi Normal University, Nanchang, 330022, China.
E-mail addresses: zmli@jxnu.edu.cn (Z.-M. Li), whuichem@126.com (W. Hui), djtao@jxnu.edu.cn (D.-J. Tao).

https://doi.org/10.1016/j.cej.2025.160639
Received 19 November 2024; Received in revised form 13 February 2025; Accepted 13 February 2025
Available online 13 February 2025

[17–19], and organic polymers [20]. However, most advanced adsorbents suffer from intrinsic rigidity, insolubility, or brittleness, which limits their application in the PSA.

As a compromise, common methods involve impregnating or coating active components onto solid surfaces to improve the adsorption performance of molded materials. However, these techniques are not without limitations, including limited adsorption capacity and poor coating stability [20–22]. In contrast, polyhydroxy compounds with strong binding affinity have proven to be as promising candidates for improving the moldability of adsorbents [23]. For example, Xing et al. demonstrated that using polyvinyl butyral (PVB) as a binder to mold anion-pillared ultramicroporous MOFs into pellets could increase the C_2H_2/C_2H_4 selectivity after pelletization [24]. Inspired by this approach, pelletizing DSLS powder with suitable binders can achieve both high adsorption performance and enhanced mechanical strength and moldability, which is of considerable significance for improving the separation efficiency of NH_3 from exhaust gases.

Herein, we successfully prepared a series of DSLS pellets via the wet pelletization process. The NH_3 adsorption performance was evaluated by varying binder types and dosages, and density functional theory (DFT) and natural bond orbital (NBO) were used to study the adsorption mechanism of SLS before and after demethylation. Furthermore, the adsorption kinetics were analyzed based on the diffusion time constants correlated with Fick's diffusion model. Moreover, the thermodynamic parameters of DSLS pellets were estimated by establishing the relationship between temperature and NH_3 adsorption behavior. Finally, the NH_3 separation selectivity, breakthrough tests, reusability, pellet size and compressive strengths were investigated to validate the separation performance of DSLS pellets for industrial PSA applications.

2. Experimental section

2.1. Materials

Anhydrous lithium bromide (99.99 %) and hydrobromic acid (48 wt %) were purchased from Shanghai Adamas Reagent Co., Ltd. Sodium lignosulfonate (SLS, 96 %), hydroxyethyl cellulose (1000–1500 mpa.s) and carboxymethyl cellulose (200–500 mpa.s) were obtained from Shanghai McLean Biochemical Technology Co., Ltd. Polyvinyl alcohol (97.0 %) and anhydrous ethanol (98 %) were purchased from Shanghai Aladdin Biochemical Technology Co., Ltd. NH_3 (99.999 %), N_2 (99.999 %), CO_2 (99.999 %), and $NH_3/CO_2/N_2$ mixture (1/1/98, v/v) were purchased from Jiangxi Huahong Special Gases Co., Ltd. These chemicals were used without additional purification.

2.2. Preparation of DSLS

The preparation method for DSLS is similar to our previously reported work [8]. In detail, 6.1 g of lithium bromide and 3.9 g of water were added into the inner chamber of a hydrothermal reactor. The mixture was stirred for 2 min until the lithium bromide was fully dissolved. Subsequently, 0.5 g of SLS was added and dissolved into the above solution. Meanwhile, 1 mL of concentrated hydrogen bromide (1.48 g, 48 % w/w) was added to achieve a final lithium bromide concentration of 53 %. The reaction mixture was then heated to 373 K and maintained at this temperature for 4 h. After the reaction, the precipitate was separated by centrifugation and washed successively with ethanol solution and deionized water. Finally, the dark black solid was freeze-dried to yield DSLS.

2.3. Preparation of DSLS pellets

The structures of PVA, HEC, or CMC binders are presented in Fig. S1. The preparation of DSLS pellets via binders with DSLS powder is described in Scheme 1. Specifically, 0.5 g of a 5 wt% PVA solution was combined with 0.475 g of degassed DSLS powder in a mortar and small quantities of distilled water were added to achieve a uniform mixture, resulting in a black agglomerate with a specific viscosity. The agglomerate was then shaped into strips and pelletized using a pellet-rolling plate, forming homogeneous spherical pellets with a diameter of ~1.9 mm. The pellets were placed in a vacuum drying oven at 333 K for 24 h, obtaining 95% DSLS@PVA pellet. The remaining two adsorbent pellets were manufactured following the procedures described above and named 95% DSLS@HEC and 95% DSLS@CMC pellets, respectively. Additionally, the 90% DSLS@PVA pellet adsorbent was obtained by changing the binder dosage to 10 wt%.

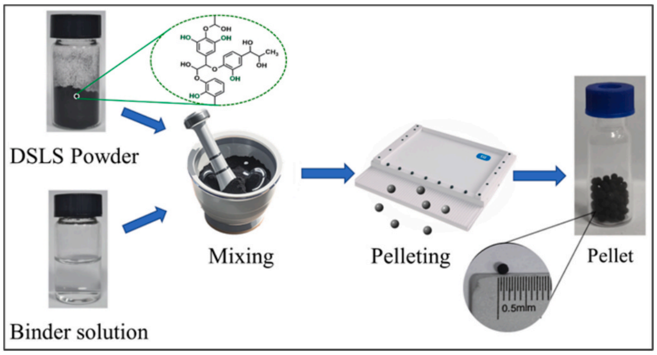

Scheme 1. DSLS pellets molding process.

2.4. Characterizations

The Fourier transform infrared spectrometer (FT-IR) spectral analysis of the samples was carried out using a Nicolet 6700 spectrometer (Therm Fisher Scientific Corporation, USA), with a scanning range of 400 to 4000 cm^{-1}. X-ray photoelectron spectroscopy (XPS) on an AXIS SUPRA instrument (Shimadzu Corporation, Japan) was used to characterize the elemental composition of the samples. The surface morphology and structure of the samples were examined via scanning electron microscope (SEM) using an S-3400 N model (Hitachi Corporation, Japan). The elemental compositions of the samples were analyzed using an EA3000 organic elemental analyzer (EuroVector Corporation, Italy) to quantify the content of C, H, and O elements. The N_2 adsorption–desorption experiment and specific surface area measurements were conducted at 77 K using a Micromeritics TriStar II 3020 analyzer (Micromeritics Instrument Corporation, USA). The compressive strengths of the pellets were tested on the KQ-3 automatic particle strength analyzer (Guorui Analytical Instruments Corporation, China). The adsorption experiments were performed at 298.2 K under a pressure range of 0 to 101.3 kPa, with all samples pre-activated under vacuum at 333 K for 24 h. The phenolic hydroxyl contents (F_{Ph-OH}) were determined using the Folin-Ciocalteu (FC) reagent method, the samples were reacted with the FC reagent under basic conditions to produce a colored complex, and the absorbances were measured at 760 nm using a U-3310 UV–Vis spectrophotometer (Hitachi Corporation, Japan).

2.5. Adsorption experiment and breakthrough test

The apparatus employed for the adsorption experiments (Fig. S2), and the column breakthrough equipment (Fig. S3) are elucidated in the Supporting Information. Detailed experimental procedures are described in the Supporting Information. The primary materials utilized for adsorption were as follows: DSLS powder, 95% DSLS@PVA pellets, 95% DSLS@HEC pellets, and 95% DSLS@CMC pellets. The breakthrough performance of the adsorbent was evaluated using a mixture of gases (1 % NH_3, 1 % CO_2, 98 % N_2) at 303 K. Before the experiment, the samples were degassed at 333 K for 24 h under a vacuum.

2.6. Abrasion test and cyclic experiment

The abrasion experimental method is as follows: a total of 100 adsorbent pellets with regular shapes and uniform smooth surfaces were selected and loaded into a YXQM-1L planetary grinder. The pellets were rotated in the forward direction at a speed of 200 rpm min^{-1}. The wear rate of the adsorbent pellet was then calculated using equation (eq.) 1 [22].

$$Cl = \frac{m_0 - m_1}{m_0} \times 100\% \tag{1}$$

Where Cl is the cumulative mass loss, m_0 is the initial mass of the adsorbent pellet (g), and m_1 is the mass of the residual adsorbent pellet (g) after the experiment.

The cyclic experiment method is as follows: The adsorbent was placed at 353 K and regenerated at 0.1 kPa for 2.5 h to obtain a regenerated adsorbent pellet. Subsequently, the pellet is regenerated and reused for NH_3 adsorption, repeating the above process to test the reversibility of the pellet material.

3. Results and discussion

3.1. Characterization

The phenolic hydroxyl contents (F_{Ph-OH}) in SLS and DSLS samples were determined using the Folin-Ciocalteu reagent method [25]. Elemental analysis was carried out to evaluate the elemental composition of each sample. The results are summarized in Table 1. It can be observed that the F_{Ph-OH} content in DSLS sample is 2.52 mmol g^{-1}, which is significantly higher than that of SLS sample (1.06 mmol g^{-1}). This differential result provides evidence for the successful demethylation of SLS sample. Meanwhile, the elemental analysis reveals that DSLS sample has reduced C content and elevated O content compared to SLS sample. This finding confirms the increase in phenolic hydroxyl groups and supports the expected reduction in methyl ($-CH_3$) groups after demethylation. Moreover, the reduction in H content in DSLS sample is consistent with this interpretation, further validating the effectiveness of the demethylation reaction.

Moreover, the chemical changes associated with the demethylation of SLS to DSLS were analyzed by FT-IR spectroscopy (Fig. 1a). In SLS and DSLS spectra, the broad adsorption peaks at 3440 cm^{-1} can be ascribed to the O-H stretching vibration of the alcohol hydroxyl and phenolic hydroxyl groups [26]. In addition, the vibrational frequency of the aromatic skeleton is increased after SLS sample is demethylated, which leads to a blue shift of the C–C/C=C stretching vibrations from 1592 cm^{-1} to 1629 cm^{-1} [27]. Additionally, the differences in peak shape at 1548 to 1218 cm^{-1} (pink color-block in Fig. 1a) correlate with $-CH_3$ groups removal, which triggers a reduction in the content of soluble sodium salts in DSLS sample [28], as evidenced by complementary XPS analysis (Fig. S4). Overall, these findings align with the significant increase in F_{Ph-OH} values shown in Table 1, which corroborates that the demethylation reaction of SLS sample led to the formation of additional phenolic hydroxyl groups in DSLS sample.

Subsequently, the structural and morphological influences of binder types on the pelletized DSLS@binder samples were investigated by FT-IR and SEM (Fig. 1b and Fig. 2). As anticipated, the characteristic spectral adsorption bands of pelletized DSLS@binder closely resembled those of powdered DSLS. FT-IR results suggest that the low dosages (5 wt %) of the binder have a negligible effect on the structural integrity of the pelletized adsorbents, which means that the active sites necessary for NH_3 separation are well retained during the pelletization process. Furthermore, SEM images revealed that pure DSLS powder exhibited irregular polymer-like aggregates, which were partially stacked into larger aggregates under the action of PVA, HEC and CMS binders. These results imply that the binder exhibits suitable bonding ability for the moldability of pelletized adsorbents. As a result, it ensures powdered DSLS samples can be molded into a specific shape of DSLS@binder adsorbents and used for NH_3 adsorption in PSA. TG analysis shows that DSLS powder and the 95% DSLS@PVA pellets undergo dehydration in the range of 298–373 K and pyrolysis onset temperature at about 460 K (Fig. S5). In addition, the pyrolysis temperature of DSLS@PVA is slightly higher than that of pure DSLS, indicating that the incorporation of the binder improved the thermal stability of the pelletized adsorbents.

Table 1
Phenolic hydroxyl groups and elemental analysis of SLS and DSLS samples.

Sample	F_{Ph-OH} (mmol g^{-1})	Elemental analysis				
		C (wt %)	H (wt %)	O (wt %)	N (wt %)	Others (wt %)
SLS	1.06	38.69	4.90	51.76	0.73	3.92
DSLS	2.52	36.73	4.57	54.88	0.79	3.02

3.2. Adsorption performance and mechanism

The NH_3 adsorption performance of powdered and pelletized adsorbents was evaluated at 298.2 K and 101.3 kPa. As shown in Fig. 3a, the demethylation of SLS confers a remarkable improvement in NH_3 capture capacity of DSLS. As a result, DSLS achieves a 577.4% increase over SLS (11.5 *vs.* 1.7 mmol g^{-1}). Moreover, DSLS shows a satisfactory fast NH_3 adsorption rate, which reaches saturation capacity of 71.3% (8.2 mmol g^{-1}) within 0.5 min (30 s) and achieves an adsorption equilibrium within 10 min. This dramatic performance improvement stems from acidic phenolic hydroxyl groups (Ph−OH) present in DSLS sample, which serve as high-performance active sites for NH_3 capture. Fig. 3b and Table 2 show the effect of binder dosages on the pelletized DSLS@PVA adsorbents. The results indicate that 95% DSLS@PVA has superior low-pressure NH_3 adsorption capacity and near-ideal performance retention across the entire pressure range (0–101.3 kPa). The control experiments with pure PVA, HEC, and CMS binders confirm that their contribution to NH_3 adsorption performance is negligible (Fig. S6). Specifically, based on the mass ratio of 95:5 for DSLS to binders, the theoretical contributions to NH_3 adsorption in DSLS@binder adsorbents are estimated to be about 0.13 mmol g^{-1} (PVA), 0.14 mmol g^{-1} (HEC) and 0.18 mmol g^{-1} (CMC), which mean that DSLS is the dominant active site.

In addition, the optimized 95% DSLS@PVA has an NH_3 adsorption loss of 2.3% compared with powdered DSLS. However, the binder dosages were further increased to 15 wt% (85% DSLS@binder) reduces NH_3 capacity to ~9 mmol g^{-1} (Fig. S7). Moreover, when the binder dosage is tuned to 10 wt% (90% DSLS@PVA), the NH_3 adsorption isotherm to linear behavior, which indicates the loss of its advantage in low-pressure adsorption ability (Fig. 3b). These results can be attributed to the fact that the higher binder dosage can cover or block the active sites, leading to a more linear adsorption behavior. It is worth noting that the adsorbent exhibits a denser packing structure after molding, as confirmed by SEM. Therefore, it can be inferred that the reduction in NH_3 uptake for the DSLS@PVA adsorbents are primarily attributed to increased internal gas diffusion resistance, which restricts NH_3 adsorption efficiency. Alos, this result suggests that the delicate balance between binder dosage and active site accessibility is required in optimizing the NH_3 adsorption performance of pelletized adsorbents. Next, the comparative analysis of various binders with different functional groups demonstrated that PVA has a minimal impact on the low-pressure NH_3 uptake of the pelletized adsorbents (Fig. 3c, 3d and Table 2). It was found that 95% DSLS@PVA consistently outperformed the other binder formulations under increasing pressure conditions, which suggests that PVA improved DSLS moldability and its NH_3 adsorption capacity was closer to that of DSLS. Therefore, based on the study of the effects of various binder types and dosages on pelletization in the mentioned experiments, PVA was selected as the binder for pelletization of DSLS, which showed the minimal impact and the optimal NH_3 capture efficiency in terms of NH_3

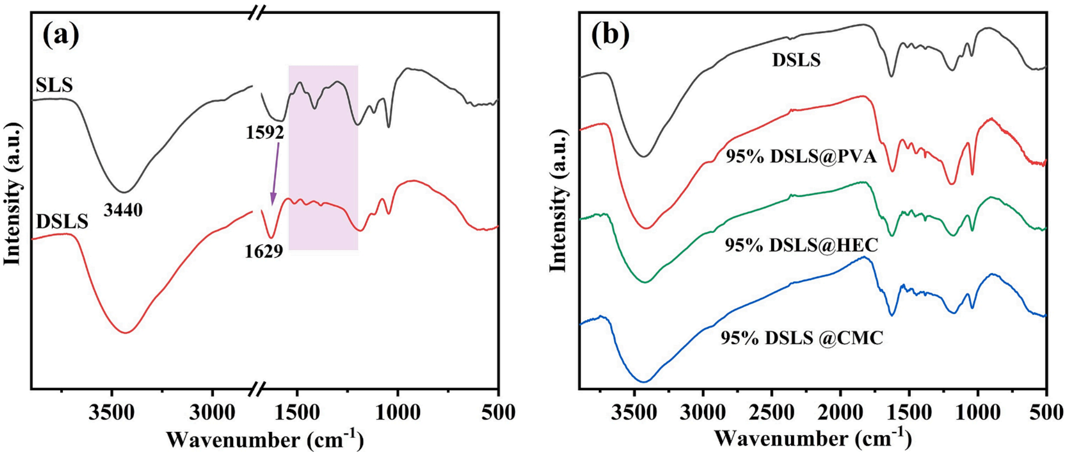

Fig. 1. FT-IR spectra of (a) powdered SLS, DSLS samples, and (b) DSLS and pelletized DSLS@binder samples.

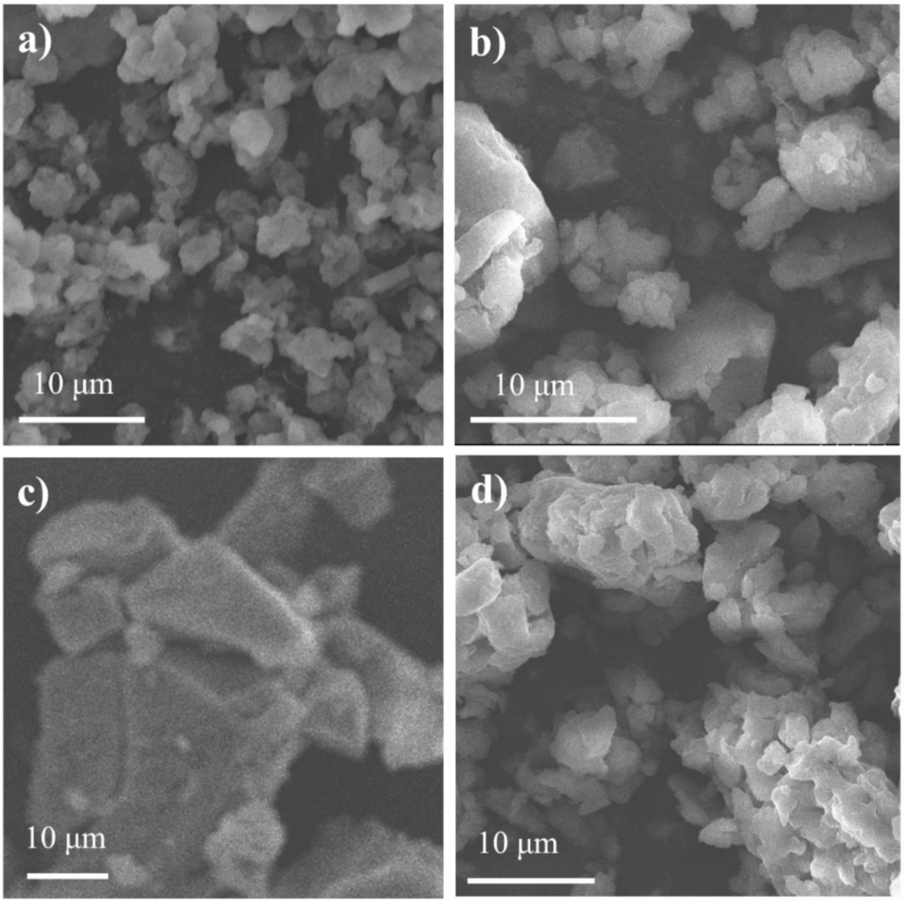

Fig. 2. SEM images of (a) DSLS powder, (b) 95% DSLS@PVA, (c) 95% DSLS@HEC and (d) 95% DSLS@CMC samples.

separation at low-pressure conditions.

In addition, DFT calculations were used to study the mechanism underlying the differences in the gas adsorption performance before and after SLS demethylation. First, the binding energies of the three gases with SLS and DSLS were analyzed (Table 3). The data indicates that SLS exhibits strong adsorption for both CO_2 and NH_3, with adsorption energies of -25.48 kJ mol^{-1} and –22.82 kJ mol^{-1}, respectively, while the adsorption energy for N_2 is the lowest at -2.94 kJ mol^{-1}. This suggests a strong affinity of SLS for NH_3 and CO_2. After demethylation, the adsorption energy of NH_3 on DSLS increases significantly to -73.77 kJ mol^{-1}, whereas the energy for CO_2 decreases to -12.58 kJ mol^{-1}, and that for N_2 slightly decreases to -2.49 kJ mol^{-1}. These findings demonstrate that SLS demethylation enhances NH_3 adsorption while substantially reducing the adsorption of CO_2 and N_2, thereby improving the selectivity for NH_3. This trend is consistent with experimental results.

Subsequently, the interactions between the two types of SLS and gas molecules were systematically investigated. The optimized structures of SLS, DSLS (Fig. 4a and 4b), and their respective interactions with NH_3 are presented in Fig. 4c and 4d. Prior to demethylation, the interaction

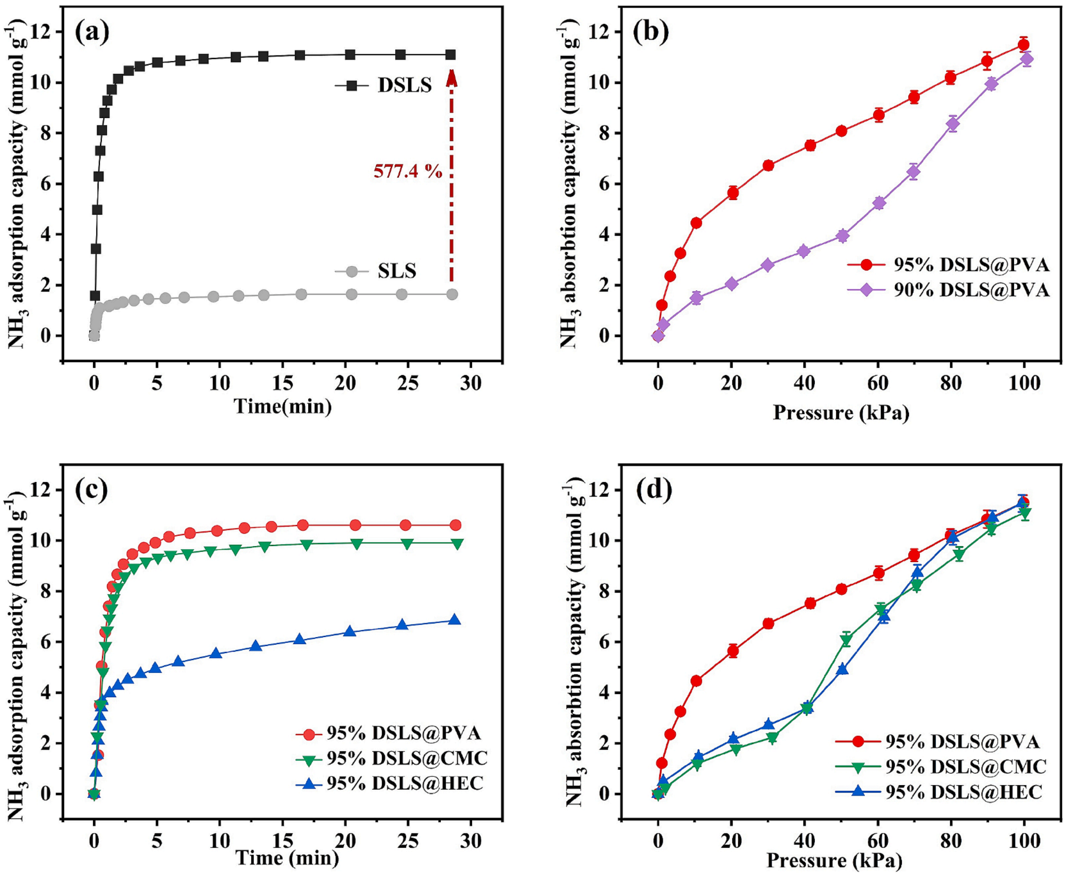

Fig. 3. (a) The NH$_3$ adsorption rate curves of (a) SLS and DSLS powder (b) NH$_3$ adsorption isotherms of DSLS@PVA with different dosage (c) NH$_3$ adsorption rate curves of 95% DSLS@binder and (d) NH$_3$ adsorption isotherms of 95% DSLS@binder samples at 298.2 K and 101.3 kPa.

Table 2
The NH$_3$ adsorption capacity of powder and pellets based on isotherms at 298.2 K and 101.3 kPa.

Samples	NH$_3$ uptake (mmol·g^{-1})			Uptake loss (per gram DSLS)
	1 kPa	10 kPa	101.3 kPa	
DSLS powder	2.33	5.22	12.26	–
95% DSLS@PVA pellet	1.20	4.46	11.50	2.3 %
95% DSLS@HEC pellet	0.48	1.49	11.40	3.3 %
95% DSLS@CMC pellet	0.25	1.18	11.12	6.0 %

Table 3
The binding energies and their ratios of the samples with the adsorbed gases.

Samples	Guest gases			Binding energy ratios	
	NH$_3$ (kJ mol^{-1})	CO$_2$ (kJ mol^{-1})	N$_2$ (kJ mol^{-1})	NH$_3$/CO$_2$	NH$_3$/N$_2$
SLS	−22.82	−25.48	−2.94	0.90	7.76
DSLS	−73.77	−12.58	−2.49	5.86	29.61

between SLS and NH$_3$ is relatively weak, as indicated by the large intermolecular distance (Fig. 4c). Specifically, the distance between the nitrogen atom (N1) in NH$_3$ and the nearest hydrogen atom (H4) in SLS extends to 2.47 Å. Additionally, the C1–H4 bond length (1.09 Å) remains unchanged upon interaction with NH$_3$, confirming the absence of substantial hydrogen bonding. In contrast, in the case of DSLS (Fig. 4d), the NH$_3$ molecule is positioned much closer, with the N1–H4 distance significantly reduced to 1.52 Å. Moreover, the lengthening of the O1–H4 bond reaches 0.08 Å, suggesting the formation of a moderate hydrogen bond, which, according to Jeffrey's hydrogen bonding classification [29], almost approaches the strongly covalent type. Furthermore, for DSLS interacting with CO$_2$ or N$_2$, the hydroxyl bond length (O1–H1) remains constant at 0.97 Å after interaction (Fig. S8), indicating an absence of significant hydrogen bonding with these gas molecules.

Natural bond orbital (NBO) analysis provides an effective approach for investigating charge delocalization in hydrogen-bonded complexes. NBO analysis was then employed to probe the intermolecular interaction in greater depth. The natural population analysis (NPA) charges of all atoms in NH$_3$ within the binary complexes of SLS and DSLS with NH$_3$ are summarized in Table 4. Negligible charge transfer (ΔQ) is observed between NH$_3$ and SLS, with ΔQ as low as 0.007. In contrast, a significant charge transfer occurs for NH$_3$ and DSLS, where ΔQ reaches 0.119, highlighting the presence of a much stronger hydrogen bond interaction. Additionally, the NPA charges and ΔQ for the interactions of CO$_2$ and N$_2$ with SLS and DSLS are presented in Table S1 and Table S2. It can be observed that the Q values are all very small, indicating that the interaction between CO$_2$ and N$_2$ with SLS regardless of demethylation is very weak. To quantitatively assess the donor–acceptor interactions in hydrogen-bonded structures, the second-order perturbation approach was applied [30]. Through above analysis, it could be found the strongest interaction site of DSLS with the NH$_3$ molecule is located at the N1–H4 atoms. The stabilization energy E(2) for the interaction between the lone pair (LP) orbital of N1 and the anti-bonding lone pair orbital (LP*) of H4 reaches 99.76 kcal mol^{-1}, exhibitting the strongest donor–acceptor orbital interaction. Fig. 5b visually demonstrates the isosurface map (isovalue = 0.05 au) of valence NAOs (Natural atomic

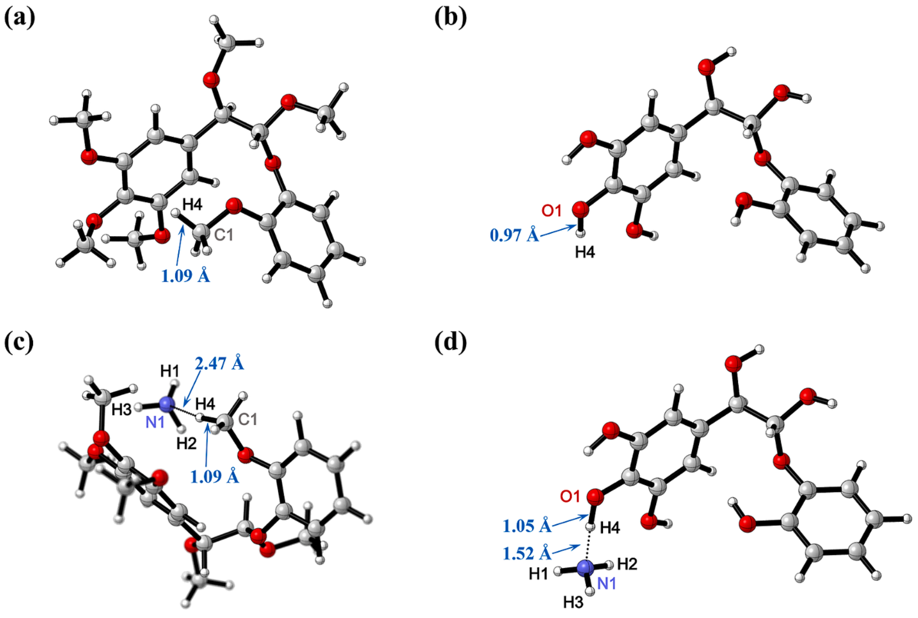

Fig. 4. Optimized structures of (a) SLS, (b) DSLS, and their corresponding interactions with NH_3: (c) SLS–NH_3 and (d) DSLS–NH_3.

Table 4
NPA charges of atoms in NH_3 within the binary complexes of SLS and DSLS with NH_3 and net charge transfer ΔQ.

Complexes	Q(N1)	Q(H1)	Q(H2)	Q(H3)	△Q(NH_3)
SLS--NH_3	−1.129	0.371	0.381	0.384	0.007
DSLS--NH_3	−1.065	0.383	0.417	0.384	0.119

Note: Q is the charge of specified atom.

orbitals) of LP(σ) N1 (composed of N($sp^{5.45}$)) and LP*(σ) H4 (composed of H(s)). It can be observed that these two orbitals exhibit a highly distinct overlap. This extensive orbital overlap suggests strong electron delocalization, which is the fundamental reason behind the prominent hydrogen bonding between DSLS and NH_3. Differently, the interaction between SLS and NH_3 is markedly weaker. The strongest donor–acceptor interaction occurs between the LP orbital of N1 (composed of N($sp^{12.10}$)) and the anti-bonding orbital BD*(C1–H4) (composed of 0.6200C($sp^{2.75}$)-0.7864H(s)), with the largest stabilization energy E(2) of only 2.28 kcal mol^{-1}. Fig. 5a shows that these two orbitals exhibit a noticeable gap, indicating poor electron delocalization and thus an extremely weak interaction between SLS and NH_3.

3.3. Adsorption kinetic analysis

The time-dependent NH_3 adsorption kinetics of DSLS and DSLS@binder were analyzed through the Fick diffusion model (eq. (2)) [31,32]. The model fitting was conducted on data exceeding 70 % of the adsorption capacity to exclude the confounding factors of initial chemical-physical adsorption, thereby providing a more accurate representation of diffusion-dominated kinetics.

$$1-\frac{m_t}{m_{max}}=\frac{6}{\pi^2}\exp\left(\frac{-\pi D_c t}{r_c^2}\right) \tag{2}$$

where m_t is the NH_3 uptake at time, m_{max} is the uptake capacity of NH_3 when adsorption equilibrium is reached. D_c is the diffusion coefficient of the gas in the adsorbent, r_c is the equivalent radius of the adsorbent, D_c/r_c^2 is the diffusion time constant.

As shown in Fig. 6, the fitted normalized curves demonstrate goodness-of-fit ($R^2 > 0.91$), which indicates that the Fick diffusion model accurately describes the NH_3 adsorption kinetics of both DSLS and DSLS@binder samples [33]. The calculated diffusion coefficients show differences between samples, which implies variations in internal diffusion resistance due to the different binders combined with DSLS. For pure DSLS (Fig. 6a), the diffusion coefficient was found to be 0.112 min^{-1}, which reflects relatively fast NH_3 transport within the DSLS compared to DSLS@binder. In contrast, the 95% DSLS@PVA and 95% DSLS@CMC samples (Fig. 6b, 6c) exhibited similarly lower diffusion coefficients (about half of pure DSLS). The results suggest that the addition of binder increases the NH_3 diffusion resistance of pelletized DSLS@binder, which is consistent with the agglomeration of adsorbent

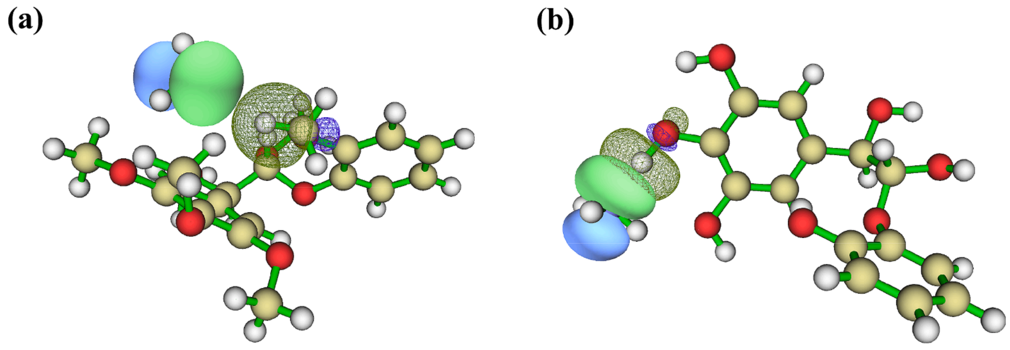

Fig. 5. Isosurface map (isovalue = 0.05 au) of valence NAOs of (a) LP(σ) N1 and BD*(C1–H4) in SLS--NH_3, (b) LP(σ) N1 and LP*(σ) H4 in DSLS--NH_3.

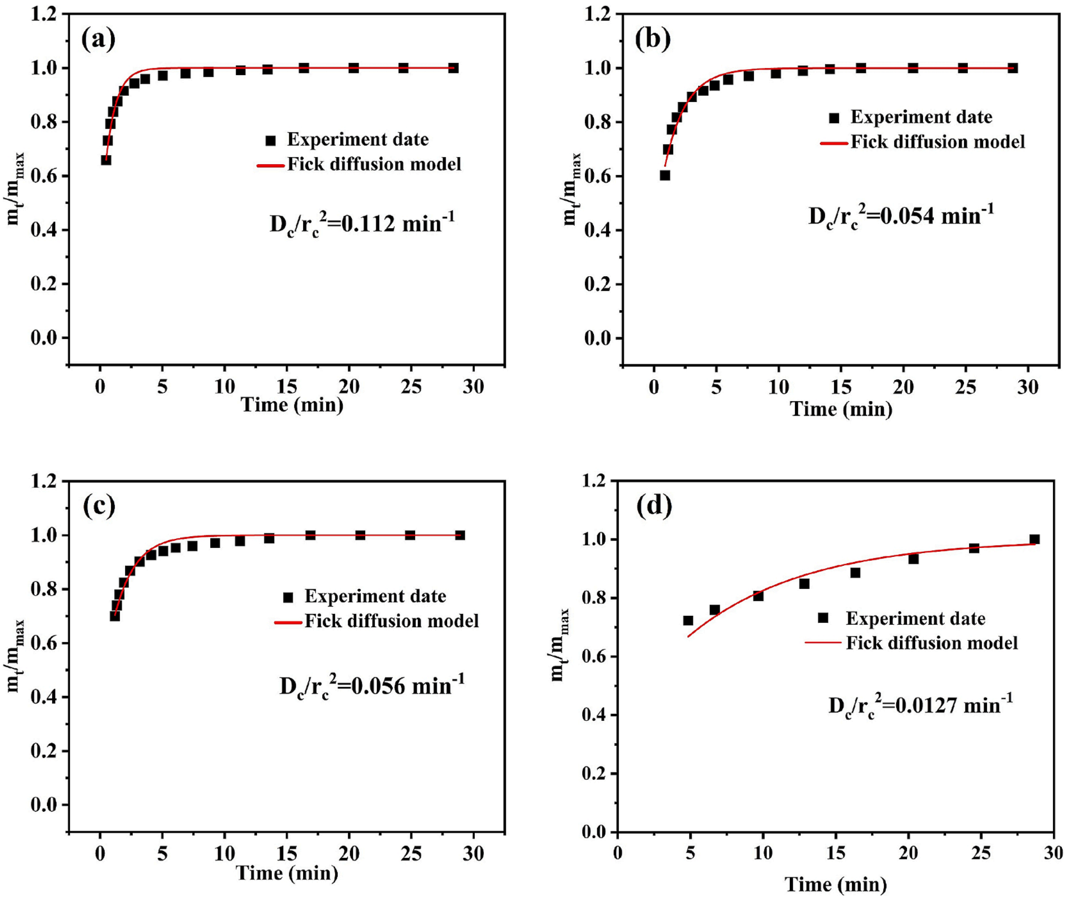

Fig. 6. Fitting curves of the Fick diffusion model for (a) DSLS, (b) 95% DSLS@PVA, (c) 95% DSLS@CMC, and (d) 95% DSLS@HEC samples.

pellets shown by SEM. This reduction in diffusion coefficient due to binder addition implies a potential trade-off between the mechanical properties provided by the binder and the adsorption kinetics. In particular, the 95% DSLS@HEC sample has the lowest diffusion coefficient, possibly due to interactions between its carboxyl groups and DSLS, which significantly increase the tortuosity of the diffusion pathway (Fig. 6d). Therefore, the pelletized 95% DSLS@PVA is suitable for applications requiring rapid adsorption. On the other hand, the 95% DSLS@HEC may be more appropriate for applications where controlled diffusion rates are beneficial..

3.4. Thermodynamic analysis

The adsorption isotherms of 95% DSLS@PVA sample were tested at 298.2 K, 318.2 K and 338.2 K to elucidate the effect of temperature and pressure on NH_3 adsorption (Fig. 7a). The results show that NH_3 adsorption capacities increase nonlinearly with rising pressure at all temperatures, while the NH_3 adsorption capacities decrease with increasing temperature. The above-mentioned trend suggests that NH_3 adsorption is an exothermic process, where higher temperature weakens the binding affinity of the Ph−OH active sites to NH_3 molecules via destabilizing the interactions between adsorbent and adsorbate. In parallel, adsorbent analyses were carried out using empirical equations (eqs. 3–5) to dissect the total adsorption into chemical and physical adsorption [34]. The fitted curve for the adsorption of NH_3 on 95% DSLS@PVA pellet is shown in Fig. 7b, and the corresponding parameters are listed in Table S3. It can be observed that chemisorption dominates at 0–20 kPa, as evidenced by the rapid initial ascent of the adsorption capacity. This dominance of chemisorption can be attributed to the interaction of NH_3 with Ph−OH groups on 95% DSLS@PVA. However, the adsorption isotherm changes to a near-linear pressure dependence at 20–101.3 kPa, which indicates that physisorption is becoming the predominant mechanism while chemisorption approaches a plateau. Moreover, the fact that $R^2 > 0.99$ further supports the high reliability of the model. Besides, the NH_3 adsorption isotherm of 95% DSLS@PVA at 298.2 K was fitted using the Langmuir and Freundlich models, with the results shown in Fig. S9. It can be found that the Freundlich model ($R^2 = 0.99$) more accurately describes the adsorption process than the Langmuir model ($R^2 = 0.96$), which implies that the adsorption sites of 95% DSLS@PVA are uneven [35]. Also, the results suggest that NH_3 adsorption behavior of 95% DSLS@PVA is multilayer adsorption, which is consistent with the coexistence of distinct chemisorption and physisorption. In short, these results suggest that the synergistic adsorption of 95% DSLS@PVA is the key to efficient NH_3 separation, where chemisorption provides a fast NH_3 adsorption rate and selectivity at low pressures, and physisorption increases NH_3 capacity at higher pressures.

$$\mathscr{X} = \mathscr{X}_R + \mathscr{X}_H = \mathscr{X}_e \frac{KP}{1+KP} + \frac{P}{H} \tag{3}$$

$$\mathscr{X}_R = \mathscr{X}_e \frac{KP}{1+KP} \tag{4}$$

$$\mathscr{X}_H = \frac{P}{H} \tag{5}$$

Where $\mathscr{X}$ is the total adsorption capacity of the sample for NH_3, including $\mathscr{X}_R$ is chemical adsorption capacity and $\mathscr{X}_H$ is physical adsorption capacity, $\mathscr{X}_e$ is the maximum adsorption capacity for chemical adsorption, K is the adsorption equilibrium constant for the reaction, and H is Henry's constant.

Subsequently, thermodynamic analyses were performed using eqs. (6) and (7) to calculate the equilibrium constant (K) and Henry's

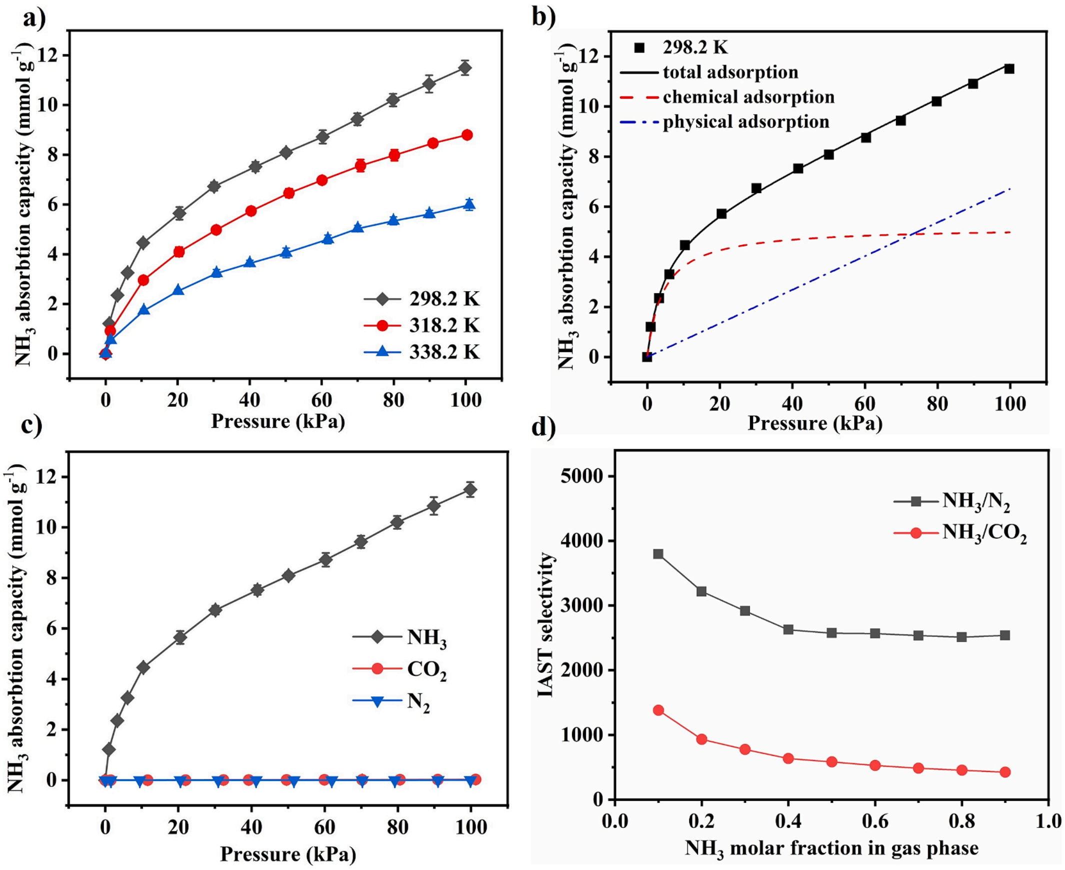

Fig. 7. (a) The NH_3 adsorption isotherms of 95% DSLS@PVA at different temperatures, (b) the fitted curves (c) the adsorption isotherms of 95% DSLS@PVA for NH_3, N_2, and CO_2 at 298.2 K and 101.3 kPa, and (d) the separation selectivity at varying pressures on 95% DSLS@PVA samples.

constant (H). The linear fits of ln K versus 1/T (Fig. 8a) and ln H versus 1/T (Fig. 8b) reveal a strong temperature correlation. The calculated chemisorption enthalpy ($\Delta H_{chem} = -31.13$ kJ·mol^{-1}) is notably lower than that of most NH_3 adsorbents reported in the literature [13,36], which means that a moderate binding energy reflects an optimal balance between suitable chemical interaction and manageable regeneration energy requirements. Meanwhile, the calculated physisorption enthalpy ($\Delta H_{phy} = -19.6$ kJ·mol^{-1}) indicates weaker Van der Waals interactions, which enable rapid capture and release of NH_3 under mild conditions.

$$\frac{\partial lnK}{\partial(1/T)} = -\frac{\Delta H_{chem}}{R} \tag{6}$$

$$\frac{\partial lnH}{\partial(1/T)} = -\frac{\Delta H_{phy}}{R} \tag{7}$$

3.5. *IAST selectivity and breakthrough curves*

The ability of pelletized adsorbents to selectively capture NH_3 in the presence of competing gases (e.g., CO_2 and N_2) is crucial for industrialization. The adsorption performance of 95% DSLS@PVA pellets was

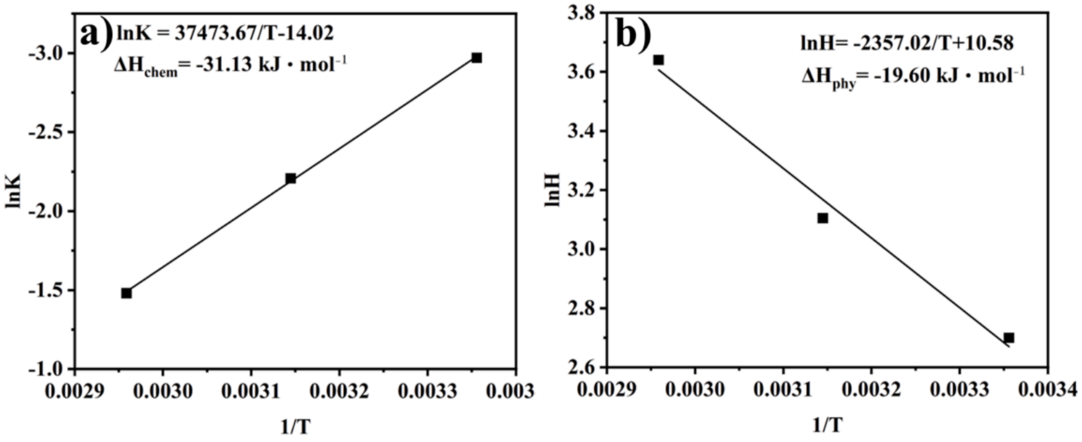

Fig. 8. The linear fits of (a) lnK and 1/T and (b) lnH and for NH_3 adsorption on 95% DSLS@PVA samples.

assessed for NH_3, CO_2 and N_2 at 298.2 K and 101.3 kPa (Fig. 7c). The results show that 95% DSLS@PVA selectively adsorbs NH_3 compared to other gases under the same conditions, while its shows almost negligible adsorption of CO_2 and N_2. Next, the gas selectivity metrics were quantified using the Ideal Adsorbed Solution Theory (IAST) method, and the result is shown in Fig. 7d. The selectivity values for NH_3/CO_2 (10/90, v/v) and NH_3/N_2 (10/90, v/v) reached 1380 and 3753, respectively. These results can be attributed to the presence of active sites (Ph−OH) on 95% DSLS@PVA that preferentially bind NH_3, coupled with the reduced specific surface area due to binder incorporation, which suppresses physisorption of CO_2 and N_2. In addition, a comparison of 95% DSLS@PVA pellets with similar NH_3 adsorbents revealed that the NH_3 adsorption capacity of 95% DSLS@PVA is highly competitive among similar adsorbent materials, especially considering cost and sustainability, and the comparative results are presented in Table S4.

To simulate practical conditions, column breakthrough experiments were carried out with a ternary gas mixture (1 % NH_3, 1 % CO_2, 98 % N_2) at 303 K and a flow rate of 30 mL·min^{-1} (Fig. 9a). The breakthrough curves show that NH_3 is retained for up to 370 min g^{-1}, which is well above the breakthrough times for CO_2 and N_2. Furthermore, integration of the breakthrough curves gave a dynamic adsorption capacity of 2.07 mmol·g^{-1} for NH_3. Therefore, the thermodynamic and IAST selectivity analysis shows chemisorption contributed by Ph−OH groups plays a dominant role in the selective capture of NH_3, while physical adsorption helps to maintain the capacity over a longer period.

3.6. *Mechanical stability and reusability*

Mechanical stability is a critical parameter for solid adsorbents in industrialization, where wear resistance under continuous cycling determines long-term operational suitability. Firstly, the pellet sizes of the 95% DSLS@PVA were measured to ensure the accuracy of the mechanical strength tests (Fig. S10a). The results show that 79.87 % of the pellet sizes were within 2 ± 0.1 mm or 2 ± 0.2 mm, with an average diameter of ~1.96 mm. Next, the wear resistance of 95% DSLS @PVA pellets was tested to evaluate mechanical durability. As illustrated in Fig. 9b, the cumulative mass loss rate of the 95% DSLS@PVA pellets showed a minor increase, from 3.52 % after 12,000 rotations to 4.31 % after 24,000 rotations. In addition, the free-fall (1 m height) drops test and compressive strength test demonstrated that 95% DSLS@PVA adsorbent had excellent impact resistance and compressive strength, and could withstand external applied loads in range from 16.64 N to 27.47 N (Fig. S10b). The results show the effectiveness of the PVA binder in forming compact and durable mechanical properties that ensure sustainable wear resistance in industrial-scale NH_3 capture and separation.

The industrial deployment of adsorbents requires not only mechanical stability but also sustained performance over repeated adsorption–desorption cycles. The long-term reusability of 95% DSLS@PVA sample was evaluated through nine consecutive adsorption–desorption tests at 298.2 K and 101.3 kPa. The samples were desorbed at 353 K under a vacuum of 0.01 kPa for 30 min before each cycle. Fig. 9c shows the NH_3 adsorption capacity of the 95% DSLS@PVA pellets over fresh and the next nine cycles. It is found that after the initial adsorption, the reused 95% DSLS@PVA consistently retained about 80 % of its full adsorption capacity (11.5 mmol g^{-1}) over the subsequent nine cycles. The results mean that this consistent cyclic performance during adsorption–desorption tests highlights the excellent durability and structural stability of 95% DSLS@PVA for NH_3 separation applications.

Furthermore, the FT-IR spectra of 95% DSLS@PVA FT-IR samples before and after NH_3 adsorption were compared to analyze the possible causes of incomplete NH_3 desorption. As evidenced by the FT-IR spectra

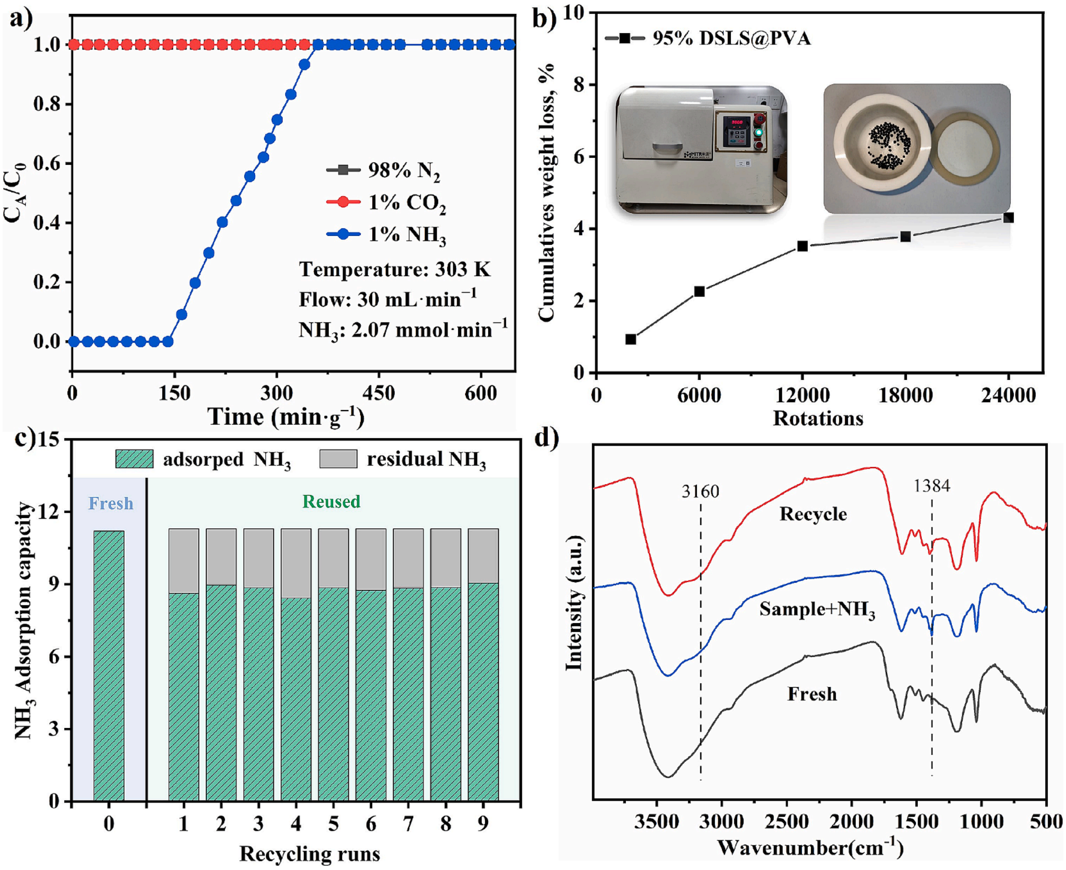

Fig. 9. (a) Column breakthrough curves, (b) the wear test, (c) cycling performance of 95% DSLS@PVA samples, and (d) FT-IR spectra of 95% DSLS@PVA samples before and after NH_3 adsorption and after cycling.

in Fig. 9d, the characteristic peaks at 1384 cm^{-1} (N-H bending) and 3160 cm^{-1} (N-H stretching) confirm the presence of residual NH_3 [16]. These NH_3 molecules are likely to remain trapped within the micropores of 95% DSLS@PVA pellets and are difficult to be completely desorbed within 30 min at 353 K and 0.01 kPa. It is inferred that the incomplete NH_3 desorption observed in the reuse tests is due to the combined effect of the interaction between Bronsted acid sites and NH_3 molecules, as well as the structural changes in the pelletized 95% DSLS@PVA adsorbent resulting from the pelletization process. In fact, this partial desorption phenomenon aligns with findings reported for similar adsorbents [37–39], where harsher desorption parameters (e.g., higher temperatures or extended times) are necessary for complete NH_3 removal. However, such conditions would increase energy consumption and operational costs. As a result, the desorption parameters in this work strike a balance between efficient NH_3 removal and practical energy use. Besides, it is worth noting that the sustained high adsorption capacity (~9 mmol g^{-1}) and mechanical stability of the 95% DSLS@PVA pellets after repeated cycles demonstrate their excellent regeneration performance and durability. Therefore, combined with the advantage of upcycling waste lignin, DSLS@PVA pellets are suitable for separation of diluted NH_3 gas, particularly in industrial operations that require sustainable and cost-effective cyclic adsorption.

4. Conclusion

In this work, we present a sustainable and industrially viable approach to valorize waste SLS into high-performance pelletized adsorbents for diluted NH_3 capture. The successful demethylation of SLS significantly increased the F_{Ph-OH} content of DSLS, enabling DSLS to achieve an exceptional NH_3 adsorption capacity of 12.26 mmol g^{-1} at 298.2 K and 101.3 kPa. In addition, the optimizations of pelletization have improves the applicability of pelletized DSLS@binder for NH_3 adsorption and separation in PSA. The optimized 95% DSLS@PVA pellets exhibited an NH_3 adsorption capacity of 11.5 mmol g^{-1} and ultrafast adsorption kinetics (half-capacity uptake time of 38 s). Moreover, the pelletized 95% DSLS@PVA demonstrates excellent IAST selectivities for the separation of NH_3/CO_2 (1380) and NH_3/N_2 (3753). The breakthrough experiment has further verified the effective separation of the $NH_3/CO_2/N_2$ (1:1:98, v/v/v) gas mixture by the 95% DSLS@PVA. In addition, the 95% DSLS@PVA also exhibits favorable mechanical stability and reusability. Therefore, we believe that pelletized DSLS@PVA adsorbents have significant potential for efficient adsorption and separation of dilute NH_3 in industrialization.

CRediT authorship contribution statement

Guo-Wen Fang: Investigation, Formal analysis. **Zhang-Min Li:** Methodology, Resources. **Jian-Fei Li:** Investigation. **Dan-Dan Cai:** Validation. **Yu-Jie Xiong:** Investigation. **Yan Zhou:** Visualization, Data curation. **Wei Hui:** Investigation, Writing – review & editing, Writing – original draft, Supervision, Funding acquisition. **Duan-Jian Tao:** Conceptualization, Funding acquisition, Project administration, Supervision, Resources.

Declaration of competing interest

The authors declare that they have no known competing financial interests or personal relationships that could have appeared to influence the work reported in this paper.

Acknowledgments

The project was financially supported by the National Natural Science Foundations of China (22378178 and 22068013), the Natural Science Foundations of Jiangxi Province (20232BAB203052 and 20242BAB20111).

Appendix A. Supplementary data

Supplementary data to this article can be found online at https://doi.org/10.1016/j.cej.2025.160639.

Data availability

Data will be made available on request.

References

[1] I. Matito-Martos, A. Martin-Calvo, C.O. Ania, J.B. Parra, J.M. Vicent-Luna, S. Calero, Role of hydrogen bonding in the capture and storage of ammonia in zeolites, Chem. Eng. J. 387 (2020) 124062.

[2] N.N. Cheng, Z.L. Li, H.C. Lan, W.L. Xu, K. Huang, Remarkable NH_3 adsorption in metal-based deep eutectic solvents by multiple coordination and hydrogen-bond interaction, AIChE J. 68 (2022) e17660.

[3] L. Luo, J. Li, X. Chen, X. Cao, Y. Liu, Z. Wu, X. Luo, C. Wang, Superhigh and reversible NH_3 uptake of cobaltous thiocyanate functionalized porous poly ionic liquids through competitive and cooperative interactions, Chem. Eng. J. 427 (2022) 131638.

[4] D.W. Kang, S.E. Ju, D.W. Kim, M. Kang, H. Kim, C.S. Hong, Emerging porous materials and their composites for NH_3 gas removal, Adv. Sci. 7 (2020) 2002142.

[5] T. Tang, J. Fei, Y. Zheng, J. Xu, H. He, M. Ma, Y. Shi, S. Chen, X. Wang, Water-soluble Lignosulfonates: Structure, preparation, and application, ChemistrySelect 8 (2023) e202204941.

[6] H.A. Maitlo, G. Maitlo, X. Song, M. Zhou, K.H. Kim, A figure of merits-based performance comparison of various advanced functional nanomaterials for adsorptive removal of gaseous ammonia, Sci. Total. Environ. 822 (2022) 153428.

[7] M. Van Damme, L. Clarisse, S. Whitburn, J. Hadji-Lazaro, D. Hurtmans, C. Clerbaux, P.F. Coheur, Industrial and agricultural ammonia point sources exposed, Nature 564 (2018) 99–103.

[8] J.F. Li, Z.M. Li, J.B. Xu, C.Y. Guo, G.W. Fang, Y. Zhou, M.S. Sun, D.J. Tao, Demethylation of waste alkali lignin for rapid and efficient ammonia adsorption, Ind. Eng. Chem. Res. 63 (2024) 3282–3289.

[9] J. Xu, Y. Lu, Z. Song, X. Chen, W. Lin, Optimal design and analysis of a liquid hydrogen and LNG coproduction system with multistage multicycle cascade refrigeration system, Int. J. Hydrogen Energ. 49 (2024) 1432–1449.

[10] K. Li, K. Zong, X. Wang, G. Cui, D. Deng, Ionic liquids and deep eutectic solvents for NH_3 adsorption and separation: a review, New J. Chem. 47 (2023) 21426–21445.

[11] M. Yu, S.J. Zeng, Z.X. Wang, Z.Y. Hu, H.F. Dong, Y. Nie, B.Z. Ren, X.P. Zhang, Protic ionic-liquid-supported activated carbon with hierarchical pores for efficient NH_3 adsorption, ACS Sustain. Chem. Eng. 7 (2019) 11769–11777.

[12] F. Zhu, Z. Wang, J. Huang, W. Hu, D. Xie, Y. Qiao, Efficient adsorption of ammonia on activated carbon from hydrochar of pomelo peel at room temperature: Role of chemical components in feedstock, J. Clean. Prod. 406 (2023) 137076.

[13] J. Xiao, Y. Zhang, T.C. Zhang, S. Yuan, Prussian blue-impregnated waste pomelo peels-derived biochar for enhanced adsorption of NH_3, J. Clean. Prod. 382 (2023) 135393.

[14] A.J. Richard, Z.J. Chen, T. Islamoglu, O.K. Farha, H.M. El-Kaderi, Heteroatom-doped porous carbons as effective adsorbers for toxic industrial gasses, ACS Appl. Mater. Inter. 14 (2022) 33173–33180.

[15] C. Shen, P. Wang, L. Shen, X. Yin, Z. Miao, NH_3 adsorption performance of silicon-supported metal chlorides, Ind. Eng. Chem. Res. 61 (2022) 8616–8623.

[16] T.T. Hu, F. Liu, S. Dou, L.B. Zhong, X. Cheng, Z.D. Shao, Y.M. Zheng, Selective adsorption of trace gaseous ammonia from air by a sulfonic acid-modified silica xerogel: Preparation, characterization and performance, Chem. Eng. J. 443 (2022) 136357.

[17] T. Yoskamtorn, P. Zhao, X.P. Wu, K. Purchase, F. Orlandi, P. Manuel, J. Taylor, Y. Li, S. Day, L. Ye, C.C. Tang, Y. Zhao, S.C.E. Tsang, Responses of defect-rich Zr-based metal-organic frameworks toward NH_3 adsorption, J. Am. Chem. Soc. 143 (2021) 3205–3218.

[18] C. Marsh, X. Han, J. Li, Z. Lu, S.P. Argent, I. da Silva, Y. Cheng, L.L. Daemen, A. J. Ramirez-Cuesta, S.P. Thompson, A.J. Blake, S. Yang, M. Schroder, Exceptional packing density of ammonia in a dual-functionalized metal-organic framework, J. Am. Chem. Soc. 143 (2021) 6586–6592.

[19] D.W. Kim, D.W. Kang, M. Kang, J.H. Lee, J.H. Choe, Y.S. Chae, D.S. Choi, H. Yun, C.S. Hong, High ammonia uptake of a metal-organic framework adsorbent in a wide pressure range, Angew. Chem. Int. Ed. 59 (2020) 22531–22536.

[20] P. Zeng, C. Zhao, C. Liang, P. Li, H. Zhang, R. Wang, Y. Guo, H. Xia, J. Sun, Comparative study on low-temperature CO_2 adsorption performance of metal oxide-supported, graphite-casted K_2CO_3 pellets, Sep. Purif. Technol. 306 (2023) 122608.

[21] X.C. Nguyen, J.H. Kang, G. Bang, K.M. Kim, C.H. Lee, Pelletized activated carbon-based CO-selective adsorbent with highly oxidation-stable and aggregation-resistant Cu(I) sites, Chem. Eng. J. 451 (2023) 138758.

[22] P. Huang, X. Wei, X. Wang, Z. Gu, Y. Guo, C. Zhao, Facile fabrication of silica aerogel supported amine adsorbent pellets for low-concentration CO_2 removal from confined spaces, Chem. Eng. J. 468 (2023) 143629.

[23] Z.X. Cui, Y.N. Feng, Y.Q. Xue, J. Zhang, R. Zhang, J. Hao, J.Y. Liu, Shape dependence of thermodynamics of adsorption on nanoparticles: a theoretical and experimental study, Phys. Chem. Chem. Phys. 20 (2018) 29959–29968.

[24] J. Zheng, X. Cui, Q. Yang, Q. Ren, Y. Yang, H. Xing, Shaping of ultrahigh-loading MOF pellet with a strongly anti-tearing binder for gas separation and storage, Chem. Eng. J. 354 (2018) 1075–1082.

[25] F. de Sousa, A. Reimann, M. Björklund Jansson, N. Nilberbrant, Estimating the amount of phenolic hydroxyl groups in lignins, 11th ISWPC, Nice, France 3 (2001) 649-653.

[26] S. Totong, P. Daorattanachai, A.T. Quitain, T. Kida, N. Laosiripojana, Catalytic depolymerization of alkaline lignin into phenolic-based compounds over metal-free carbon-based catalysts, Ind. Eng. Chem. Res. 58 (2019) 13041–13052.

[27] W.J. Zhao, X. Li, H.W. Li, X.L. Zheng, H.W. Ma, J.X. Long, X.H. Li, Selective hydrogenolysis of lignin catalyzed by the cost-effective Ni metal supported on alkaline MgO, ACS Sustain. Chem. Eng. 7 (2019) 19750–19760.

[28] H. Wang, T.L. Eberhardt, C.P. Wang, S.S. Gao, H. Pan, Demethylation of alkali lignin with halogen acids and its application to phenolic resins, Polymers 11 (2019) 1771.

[29] G. Jeffrey, An introduction to hydrogen bonding, Oxford University Press, 1997.

[30] J. Chocholoušová, V. Špirko, P. Hobza, First local minimum of the formic acid dimer exhibits simultaneously red-shifted O–H⋯O and improper blue-shifted C–H⋯O hydrogen bonds, Phys. Chem. Chem. Phys. 6 (2004) 37–41.

[31] S.I. Garcés-Polo, J. Villarroel-Rocha, K. Sapag, S.A. Korili, A. Gil, A comparative study of CO_2 diffusion from adsorption kinetic measurements on microporous materials at low pressures and temperatures, Chem. Eng. J. 302 (2016) 278–286.

[32] L. Yue, L. Rao, L. Wang, L. An, C. Hou, C. Ma, H. DaCosta, X. Hu, Efficient CO_2 adsorption on nitrogen-doped porous carbons derived from d-glucose, Energy Fuels 32 (2018) 6955–6963.

[33] X.C. An, Z.M. Li, Y. Zhou, W. Zhu, D.J. Tao, Rapid capture and efficient removal of low-concentration SO_2 in simulated flue gas by hypercrosslinked hollow nanotube ionic polymers, Chem. Eng. J. 394 (2020) 124859.

[34] N.G. Lewis, E. Yamamoto, Lignin: occurrence, biogenesis and biodegradation, Annu. Rev. Plant Physiol. 41 (1990) 455–496.

[35] T.E. Rufford, G.C.Y. Watson, T.L. Saleman, P.S. Hofman, N.K. Jensen, E.F. May, Adsorption equilibria and kinetics of methane + nitrogen mixtures on the activated carbon norit RB_3, Ind. Eng. Chem. Res. 52 (2013) 14270–14281.

[36] A.J. Rieth, M. Dincă, Controlled gas pptake in metal–organic frameworks with record ammonia sorption, J. Am. Chem. Soc. 140 (2018) 3461–3466.

[37] W.Q. Gong, M.S. Sun, J. Li, Q.P. Gong, Y.X. Fu, Y. Zhou, D.J. Tao, Efficient and selective adsorption of NH_3 by supramolecular OHP[5]-based ternary deep eutectic solvents, J. Mol. Liq. 400 (2024) 124505.

[38] J. Zhang, Y. Ma, W. Wu, Z. Cai, Y. Cao, K. Huang, L. Jiang, Carboxylic functionalized mesoporous polymers for fast, highly efficient, selective and reversible adsorption of ammonia, Chem. Eng. J. 448 (2022) 137640.

[39] D. Jung, Z. Chen, S. Alayoglu, M.R. Mian, T.A. Goetjen, K.B. Idrees, K. O. Kirlikovali, T. Islamoglu, O.K. Farha, Postsynthetically modified polymers of intrinsic microporosity (PIMs) for capturing toxic gases, ACS Appl. Mater. Inter. 13 (2021) 10409–10415.